

Emergent gravity and gravitational lensing in quantum materials

Yugo Onishi,^{1,*} Nisarga Paul,^{1,†} and Liang Fu¹

¹*Department of Physics, Massachusetts Institute of Technology, Cambridge, MA 02139, USA*

(Dated: June 13, 2025)

We show that an effective gravitational field naturally emerges in quantum materials with long-wavelength spin (or pseudospin) textures. When the itinerant electrons' spin strongly couples to the background spin texture, it effectively behaves as a spinless particle in a curved space, with the curvature arising from quantum corrections to the electron's spin orientation. The emergent gravity gives rise to the electron lensing effect, an analog of the gravitational lensing. Our work shows that novel "gravitational" phenomena generically appear in quantum systems due to nonadiabaticity, opening new research directions in quantum physics.

Introduction. — A fascinating aspect of quantum physics is the emergence of new particles and fields in systems of electrons. One example is the emergent gauge field. In a system of itinerant electrons strongly coupled to localized spins, a gauge field naturally emerges from the coupling between the electrons and the localized spins, realizing an effective magnetic field acting on the itinerant electrons [1–5]. This effective magnetic field further gives rise to the Hall effect without external magnetic fields [6–10] and flat Chern bands that mimic Landau levels [11].

In this work, we show that an effective gravitational field naturally emerges in quantum materials with long-wavelength spin (or pseudospin) textures. Specifically, when electrons are strongly coupled to localized spins, they are effectively described as spinless particles in a curved space, as depicted in Fig. 1. The curved space gives rise to an electron lensing effect, an analog of gravitational lensing [12]. The electron lensing effect becomes more significant for fast electrons than slow electrons, in contrast to the scattering due to the effects of a scalar potential.

General theory. — We consider itinerant electrons coupled with localized spins in general d -dimensions:

$$H = \frac{(\mathbf{p} - e\mathbf{A})^2}{2m} - J\mathbf{S}(\mathbf{x}) \cdot \boldsymbol{\sigma}, \quad (1)$$

where $e(<0)$, m , \mathbf{p} , $\boldsymbol{\sigma}$ are the charge, mass, momentum, and spin of the itinerant electrons, \mathbf{A} is the vector potential describing the external magnetic field, and $\mathbf{S}(\mathbf{x})$ is the localized spin at position \mathbf{x} , with normalization $|\mathbf{S}| = 1$. J is the coupling constant between the electrons and the localized spins. When J is the largest energy scale, the spin of the itinerant electrons is effectively frozen so that their spins almost always align with the local spin $\mathbf{S}(\mathbf{x})$ and can be treated adiabatically.

When J is finite, high-order terms become important. Our focus is on the low-energy effective theory up to $\mathcal{O}(J^{-1})$. To derive the low-energy Hamiltonian, we apply the unitary transformation to rotate electron's spin

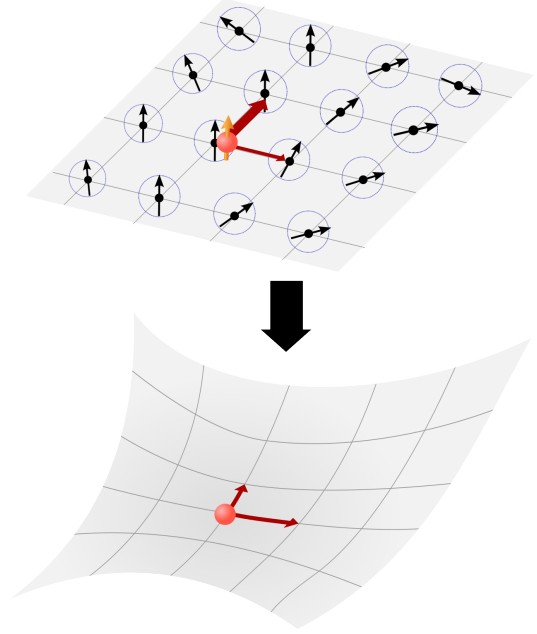


FIG. 1. Schematic illustration of emergent curved space: a spinful electron traveling through a slowly varying spin texture is equivalent to a spinless electron moving in a curved space, whose metric encodes the "stretching" of real-space distances by the spin texture.

to align with the local axis: $U^\dagger(\mathbf{x})(\mathbf{S}(\mathbf{x}) \cdot \boldsymbol{\sigma})U(\mathbf{x}) = \sigma_z$. Then the new Hamiltonian H' in the basis defined by $U(\mathbf{x})$ is

$$H' = U^\dagger(\mathbf{x})HU(\mathbf{x}) = \frac{(\mathbf{p} - e\mathbf{A} - \hbar\mathbf{a})^2}{2m} - J\sigma_z. \quad (2)$$

Here $\mathbf{a} = U^\dagger i \nabla U$ is the $U(2)$ gauge field associated with $U(\mathbf{x})$. Starting from this Hamiltonian, we will show that H' describes spinless electrons in a curved space.

Before presenting a general theory, let us consider a simple example of a spiral spin texture with wavevector \mathbf{q} , given by

$$\mathbf{S}(\mathbf{x}) = (\cos \mathbf{q} \cdot \mathbf{x}, \sin \mathbf{q} \cdot \mathbf{x}, 0) \quad (3)$$

Note that there is no emergent magnetic field since the spin texture is coplanar. In this case, we can choose the

* yugo0o24@mit.edu

† npaul@mit.edu

unitary transformation $U(\mathbf{x})$ as $U(\mathbf{x}) = \sigma_z \cos(\mathbf{q} \cdot \mathbf{x}/2) + \sigma_x \sin(\mathbf{q} \cdot \mathbf{x}/2)$ to diagonalize the spin-dependent term in Eq. (1). Notably, the resulting $U(2)$ gauge field is constant and given by $\mathbf{a} = U^\dagger i \nabla U = -\mathbf{q} \sigma_y/2$. It should be noted that \mathbf{a} *cannot* be gauged away even though it is constant, because it is a $U(2)$ gauge field, not $U(1)$. Since H' in this case is translationally invariant, it is easily diagonalized by the plane waves, and the resulting energy dispersion of the low-energy branch is

$$\begin{aligned} E(\mathbf{p}) &= \frac{p^2}{2m} + \frac{\hbar^2 \text{Tr } G}{2m} - \sqrt{J^2 + \frac{\hbar^2}{m^2} G_{ij} p_i p_j} \\ &= \frac{p_i g^{ij} p_j}{2m} + \frac{\hbar^2 \text{Tr } G}{2m} - J + \mathcal{O}(J^{-2}), \end{aligned} \quad (4)$$

where the repeated indices are summed over the spatial indices. Here, $G_{ij} = a_{12}^i a_{21}^j = q_i q_j/4$ and we have defined the *effective metric* $g^{ij} = \delta^{ij} - \hbar^2 G_{ij}/(mJ)$.

Eq. (4) and the effective metric g^{ij} show that the spin spiral suppresses the kinetic energy in the direction of \mathbf{q} at the order of $\mathcal{O}(J^{-1})$. This can be intuitively understood as the suppression of the hopping. When J is large, the spin of the itinerant electron is almost always aligned with the localized spins. When an electron hops in the direction in which the localized spin is changing, the overlap between the electron wavefunction is reduced, and hence the transfer integral of the electron is also reduced, as indicated in Fig. 1. Correspondingly, the group velocity $dE/d\mathbf{p}$ in the direction of \mathbf{q} reduces by the metric G .

The reduction of the velocity gives us a natural interpretation of the effective metric g^{ij} . Instead of viewing it as the reduction of velocity, we can interpret it as the effective length of the real space becoming longer than it actually is. The corresponding real space metric should be given by the inverse matrix of g^{ij} , which we denote by g_{ij} and is given by $g_{ij} = \delta_{ij} + \hbar^2 G_{ij}/(mJ)$ up to $\mathcal{O}(J^{-1})$. g_{ij} captures the fact that the effective length $dl \equiv \sqrt{g_{ij} dx^i dx^j}$ in the direction of \mathbf{q} becomes longer by a factor of $1 + \hbar^2 q^2/(4mJ)$.

For general spin textures, we expect that g_{ij} depends on space and thus gives rise to an effectively curved space. To derive this, we write

$$H' = \begin{pmatrix} H_1 & \Lambda \\ \Lambda^\dagger & H_2 \end{pmatrix}, \quad (5a)$$

$$H_i = \mp J + (\pi_i^2 + |\mathbf{a}_{12}|^2)/2m, \quad (5b)$$

$$\Lambda = -\{\mathbf{p} - e\mathbf{A}, \mathbf{a}_{12}\}/2m, \quad (5c)$$

with $\pi_i = \mathbf{p} - e\mathbf{A} - \mathbf{a}_{ii}$, and we treat off-diagonal terms using a Schrieffer–Wolff (SW) transformation—a unitary transformation decoupling the low and high-energy subspaces. At this point, it is useful to define three length scales: (1) $l_C = \hbar/\sqrt{mJ}$, the “Compton wavelength” associated to J (we will see that $J \sim mc^2$ in a relativistic analogy), (2) $\lambda_s = |\nabla \mathbf{S}|^{-1}$, the scale over which $\mathbf{S}(\mathbf{x})$ varies, and (3) $\lambda_F \sim \hbar/\sqrt{mE}$, the wavelength of the

electron at energy E . The SW transformation yields the following low-energy leading-order effective Hamiltonian:

$$\mathcal{H} = H_1 - \frac{\Lambda \Lambda^\dagger}{2J} \quad (6a)$$

$$= H_1 - \frac{\{\mathbf{p} - e\mathbf{A}, \mathbf{a}_{12}\} \{\mathbf{a}_{21}, \mathbf{p} - e\mathbf{A}\}}{8m^2 J}, \quad (6b)$$

which holds for *arbitrary* spin textures in the regime

$$l_C^2 \ll \lambda_s \lambda_F, \quad (7)$$

or equivalently $\langle \Lambda \rangle \ll J$ (details in Appendix A).

Furthermore, when $\mathbf{S}(\mathbf{x})$ varies sufficiently slowly such that $\lambda_s \gg \lambda_F$, the effective Hamiltonian is additionally simplified, since derivatives of $\mathbf{a}_{12}, \mathbf{a}_{21}$ are negligible compared to the other terms. In this regime, which we adopt henceforth, the effective Hamiltonian up to $\mathcal{O}(l_C^2/\lambda_s^2)$ is given by

$$\mathcal{H} = -J + \frac{\pi_i g^{ij} \pi_j}{2m} + V(\mathbf{x}), \quad (8)$$

where $g, V(\mathbf{x})$ are the effective metric and potential:

$$g^{ij} = \delta^{ij} - l_C^2 G_{ij}, \quad (9a)$$

$$V(\mathbf{x}) = \frac{\hbar^2 \text{Tr } G}{2m} - \frac{e \hbar l_C^2}{4m} \mathbf{\Omega} \cdot \mathbf{B}. \quad (9b)$$

Here G and $\mathbf{\Omega}$ are the quantum metric and the Berry curvature associated with the real space quantum geometry, respectively. These are defined with respect to the spin state of an electron aligned with the local Zeeman field at position \mathbf{R} : $(\mathbf{S}(\mathbf{R}) \cdot \boldsymbol{\sigma}) |\psi_{\mathbf{R}}\rangle = |\psi_{\mathbf{R}}\rangle$. By regarding \mathbf{R} as a parameter, we define the quantum geometric tensor Q_{ij} as

$$Q_{ij} = \langle \partial_{R_i} \psi_{\mathbf{R}} | \partial_{R_j} \psi_{\mathbf{R}} \rangle - \langle \partial_{R_i} \psi_{\mathbf{R}} | \psi_{\mathbf{R}} \rangle \langle \psi_{\mathbf{R}} | \partial_{R_j} \psi_{\mathbf{R}} \rangle \quad (10)$$

We can readily show $Q_{ij} = a_{12}^i a_{21}^j$. G and $\mathbf{\Omega}$ are then given by the real and imaginary part of Q : $G_{ij} = \text{Re } Q_{ij}$ and $\Omega^i = -\epsilon^{ijk} \text{Im } Q_{jk}$. Note that G can be written as $G_{ij} \equiv \frac{1}{4} (\partial_i \mathbf{S}) \cdot (\partial_j \mathbf{S})$. We can easily confirm that the Hamiltonian (8) reduces to Eq. (4) for spin spiral (3) with uniform metric g .

Real space quantum geometry naturally appears in the effective Hamiltonian (8) in two ways. The first is through the effective potential $V(\mathbf{x})$, whose leading $\mathcal{O}(l_C^0)$ contribution is proportional to $\text{Tr } G \propto |\nabla \mathbf{S}|^2$ [7] and corresponds to the “geometric potential” derived more generally in Ref. [13]. The subleading $\mathcal{O}(l_C^2)$ term in $V(\mathbf{x})$ represents an orbital magnetization coupling to the external \mathbf{B} field.

Interestingly, quantum geometry also manifests in a second way: through the effective metric g^{ij} . The quantum metric G_{ij} is directly realized as a correction in the spatial metric g^{ij} and thereby influences the motion of electrons. The inverse of g^{ij} , denoted by g_{ij} ,

defines the effective line element $dl = \sqrt{g_{ij} dx^i dx^j}$, and thus a spatially varying quantum metric naturally gives rise to an effective curved space and hence *emergent gravity*. The effect of the emergent gravity scales as $\mathcal{O}(l_C^2/\lambda_F^2) \sim \mathcal{O}(E_K/J)$, in close analogy with true (post-Newtonian/Einstein) gravitational effects scaling as $\mathcal{O}(E_K/mc^2)$, where E_K is the kinetic energy of a particle of mass m and c is the speed of light. Hence $J \sim mc^2$ in this analogy, which we make precise using a Lagrangian formulation in the Appendix B. [We note that the Hamiltonian for a particle in curved space can commonly take a different form: $H = g^{-1/2} p_i g^{1/2} g^{ij} p_j / (2m) + V$. This difference comes from an alternative wavefunction normalization, and we can show that the two formulations are equivalent up to $\mathcal{O}(l_C^2 \lambda_s^{-4})$ (see Appendix C for more details).]

Importantly, the emergent gravity associated to the spatial metric g gives rise to physical effects that cannot be captured by a scalar potential. This parallels how Einstein's theory of gravity goes beyond Newtonian gravity. In the following, we discuss physical consequences of the emergent gravitational field that are qualitatively new.

Gravitational lensing. — To understand the physical effects of $g(\mathbf{x})$, we analyze the classical equations of motion of the electrons, given by Hamilton's equations:

$$\dot{x}^i = \frac{\partial \mathcal{H}}{\partial p_i} = \frac{g^{ij} \pi_j}{m}, \quad (11a)$$

$$\dot{p}_i = -\frac{\partial \mathcal{H}}{\partial x^i} = -\frac{1}{2m} \pi_j \frac{\partial g^{jk}}{\partial x^i} \pi_k + \frac{e}{m} \frac{\partial A_j}{\partial x^i} g^{jk} \pi_k - \frac{\partial V}{\partial x^i}, \quad (11b)$$

where $\mathbf{A} = \mathbf{A} + (\hbar/e)\mathbf{a}_{11}$ is the total effective vector potential, including both the external and emergent gauge field. By taking the time derivative of Eq. (11a) and using Eq. (11b), we find

$$m(\ddot{x}^i + \Gamma_{jk}^i \dot{x}^j \dot{x}^k) = F^i, \quad (12)$$

where $\Gamma_{jk}^i = (g^{il}/2)(\partial_j g_{kl} + \partial_k g_{jl} - \partial_l g_{jk})$ is the Christoffel symbol with g_{ij} the inverse of g^{ij} . $F^i = g^{ij}(e\mathcal{B}_{jk}\dot{x}^k - \partial_j V)$ is the force from the potential V and the total magnetic field $\mathcal{B}_{jk} = \partial_j A_k - \partial_k A_j$. The term involving the Christoffel symbol, which scales as $\mathcal{O}(l_C^2/\lambda_F^2)$, captures the effects of the emergent gravity. Notably, the electron feels a force proportional to the square of its velocity.

In the case of a constant effective potential V and zero magnetic field \mathcal{B} , the right hand side of Eq. (12) vanishes and the equation of motion is simply the geodesic equation: $\ddot{x}^i + \Gamma_{kl}^i \dot{x}^k \dot{x}^l = 0$. Therefore, the trajectory of the electron in this case is a geodesic in the curved space. When the metric is constant, Γ_{jk}^i vanishes and the solutions are straight lines, while when the metric is spatially dependent, $\Gamma_{jk}^i \neq 0$ and thus the geodesics are no longer straight lines in general, i.e., the electron trajectory is bent by the emergent gravity. Remarkably, such trajectories are independent of the particle's initial velocity up to a rescaling of time: for a solution of the

geodesic equation $\mathbf{x}(t)$, $\mathbf{x}(\alpha t)$ for an arbitrary constant α is also a geodesic and thus a solution. Therefore, the effects of g persist even for fast-moving particles. This is in sharp contrast with the external force from a potential V , which is independent of velocity and thus affects fast-moving particles less than slow particles. This is analogous to the fact from the theory of gravity that the trajectory of light is affected by a curved space-time metric (Einstein gravity) but not by a scalar potential (Newtonian gravity).

Let us discuss perhaps the simplest consequence of the emergent gravity: the bending of electron trajectories between domains of distinct spin orders. For instance, suppose $\mathbf{S}(\mathbf{x}) = \hat{z}$ in the region $x \rightarrow -\infty$ and

$$\mathbf{S}(\mathbf{x}) = (0, \sin \frac{2\pi x}{\lambda_s}, \cos \frac{2\pi x}{\lambda_s}) \quad (13)$$

in the region $x \rightarrow +\infty$, in two spatial dimension. This describes the transition between ferromagnetic and helical domains, which could be realized for instance in a material with the Dzyaloshinskii-Moriya interaction. The emergent metric is trivially $g^{ij} = \delta^{ij}$ in the ferromagnetic region, while g^{xx} receives a correction

$$g^{xx} = 1 - (\pi l_C / \lambda_s)^2, \quad (14)$$

in the helical region. The resulting electron motion can be worked out using the conservation of energy $E = mg_{ij}\dot{x}^i \dot{x}^j / 2$ and conservation of y -momentum $p_y = mg_{yi}\dot{x}^i$. We ignore the potential V for now. This can be justified, for instance, by electrostatic gating in the helical region. Then, letting $\theta_{L/R}$ denote the angles of a geodesic with respect to the x -axis in the left and right regions, respectively, one finds that

$$\frac{\tan \theta_R}{\tan \theta_L} = \sqrt{1 + (\pi l_C / \lambda_s)^2}. \quad (15)$$

This describes the bending of electrons towards the normal as they pass from the ferromagnetic region to the helical region. In contrast with Snell's law $\sin \theta_R / \sin \theta_L = n_L / n_R$ for light, there is no condition for total internal reflection. This effect remains even in the presence of the potential V , and admits interesting generalizations, for instance to the case of domain walls between distinct spiral phases, which we discuss in the Appendix D.

Next, as a simple and solvable example, we consider the spin texture which we call the *radial spiral*

$$\mathbf{S}(\mathbf{x}) = (\cos \frac{2\pi r}{\lambda_s}, \sin \frac{2\pi r}{\lambda_s}, 0), \quad (16)$$

where $r = |\mathbf{x}|$ is the radial coordinate. Locally, the radial spiral approximately describes configurations minimizing the spin gradient energy $(\partial_i \mathbf{S})^2$ in geometries with radial boundary conditions $\mathbf{S}(r_{\min}) \neq \mathbf{S}(r_{\max})$. Globally, the radial spiral is the unique continuous, rotationally symmetric, coplanar spin texture with constant $V(\mathbf{x})$. We detail these properties in Appendix D.

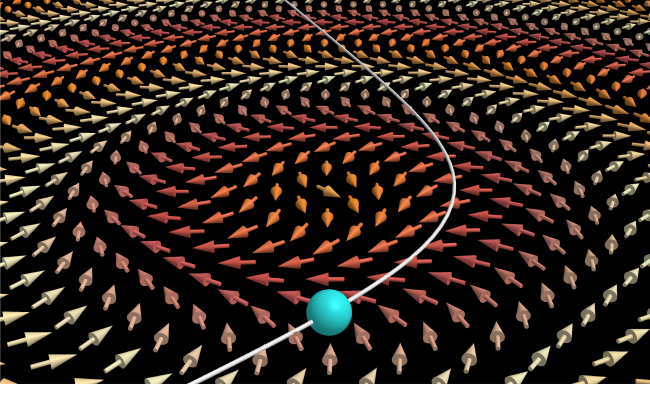


FIG. 2. The radial spiral spin texture (Eq. (16)) and a corresponding electron geodesic (solid curve). The effectively curved space gives rise to gravitational lensing of electrons around the origin.

The radial spiral is depicted in Fig. 2. It satisfies $\mathbf{b} = 0$, $V(\mathbf{x}) = \hbar^2/8m\lambda_s^2$, and

$$g^{ij} = \delta^{ij} - \left(\frac{\pi l_C}{\lambda_s}\right)^2 \frac{x^i x^j}{r^2}. \quad (17)$$

Electron motion is thus described simply by the geodesic equation, which takes the form

$$\ddot{\mathbf{x}} = -\left(\frac{\pi l_C}{\lambda_s}\right)^2 \frac{(\dot{\mathbf{x}} \times \mathbf{x})^2 \mathbf{x}}{x^4}, \quad (18)$$

indicating an $\mathcal{O}(l_C^2/\lambda_s^2)$ correction to free-particle motion. The geodesics are (writing $\nu = (\pi l_C/\lambda_s)^2$)

$$r(t) = \pm \sqrt{(v_0 t + r_0)^2 + (1 - \nu)(\hbar t/r_0)^2}, \quad (19a)$$

$$\theta(t) = \theta_0 + \frac{1}{\sqrt{1 - \nu}} (\tan^{-1}(\gamma t + \delta) - \tan^{-1} \delta) \quad (19b)$$

in polar coordinates, where $\hbar = r^2 \dot{\theta}$ is a conserved angular momentum, $(r(0), \dot{r}(0), \theta(0)) = (r_0, v_0, \theta_0)$, $\gamma = \frac{v_0^2}{\hbar \sqrt{1 - \nu}} + \frac{\hbar \sqrt{1 - \nu}}{r_0^2}$ and $\delta = \frac{r_0 v_0}{\hbar \sqrt{1 - \nu}}$. Initial conditions for geodesics are specified by r_0, θ_0, \hbar and v_0 . Alternatively, the geodesics can be expressed as straight lines in coordinates which trivialize the metric, as shown in Appendix D. An example trajectory is plotted in Fig. 2, showing clearly the *lensing* of the electron geodesic.

The properties of geodesics in the previous two examples can be elucidated by a more geometrical perspective. Quite generally, the curved space and emergent gravity in a system of d spatial dimensions corresponds to that of a surface embedded in higher dimensions. This can be seen from the effective length element $dl = \sqrt{g_{ij} dx^i dx^j}$, which can be rewritten as

$$dl^2 = d\mathbf{x}^2 + l_C^2 G_{ij} dx^i dx^j = d\mathbf{x}^2 + l_C^2 ds^2. \quad (20)$$

Here, $ds = \sqrt{G_{ij} dx^i dx^j}$ defines the quantum distance via the quantum metric G_{ij} in the local Hilbert space,

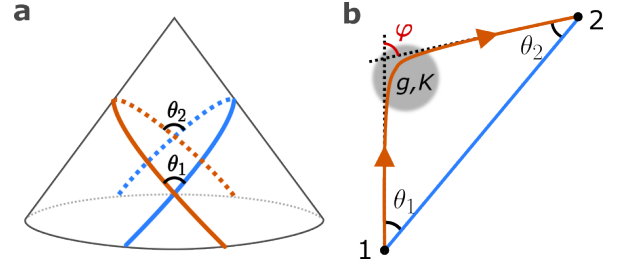


FIG. 3. (a) Two geodesics on a cone. (b) Deflection due to gravitational lensing when the curved metric and the curvature K are localized in a gray region.

which is $\mathbb{CP}^1 \simeq S^2$ in our case. Accordingly, the effective line element Eq. (20) is equivalent to that of a d -dimensional surface embedded in the $(d+2)$ -dimensional manifold, $\mathbb{R}^d \times \mathbb{CP}^1$, and l_C is the length scale associated with the extra dimensions. Eq. (20) suggests that a d -dimensional system with internal d_H -dimensional quantum degrees of freedom can naturally be viewed as living on a curved d -dimensional surface embedded in $d + d_H$ dimensions.

For coplanar textures such as $\mathbf{S}(\mathbf{x}) = (\cos \theta(\mathbf{x}), \sin \theta(\mathbf{x}), 0)$, the itinerant electron's spin is restricted to a one-dimensional subspace, and the effective curved space is a hypersurface in $d + 1$ dimensions. In particular, the effective line element can be written as

$$dl^2 = d\mathbf{x}^2 + \frac{l_C^2}{4} d\theta^2 = d\mathbf{x}^2 + dz_{\text{eff}}^2, \quad (21)$$

whose geometry is the d -dimensional surface defined by $(x^1, \dots, x^d, z_{\text{eff}}(\mathbf{x}))$ with $z_{\text{eff}} = l_C \theta(\mathbf{x})/2$.

From this geometrical perspective, the metric and geodesics of the ferromagnet-to-helical transition (Eqs. (13),(14)) correspond to the geometry of two half-planes joined at $x = 0$, with $z_{\text{eff}} = 0$ and $z_{\text{eff}} = \pi l_C x/\lambda_s$ in the left and right regions, respectively. By contrast, the metric and the geodesics of the radial spiral texture correspond to the geometry of a cone:

$$(x, y) \mapsto \left(x, y, \frac{\pi l_C}{\lambda_s} \sqrt{x^2 + y^2}\right). \quad (22)$$

Incidentally, the cone geometry Eq. (17) is the solution of the Einstein equations with a point mass M in $(2+1)$ -dimensions with the identification $(\pi l_C/\lambda_s)^2 \sim 8GM/c^2$ where G is the gravitational constant [14]. The radial spiral therefore realizes the simplest non-vacuum solution of $(2+1)$ d Einstein gravity with vanishing cosmological constant. More general spin textures will generically give rise to more complicated metrics and geodesics. We collectively refer to the ensuing new effects on electronic motion as *gravitational lensing*. Crucially, gravitational lensing becomes stronger for faster electrons and cannot be explained by an effective magnetic or electric field.

Curvature of the effective curved space is essential in the gravitational lensing effect. When the curva-

ture vanishes, the space is flat and there exist coordinates in which the trajectories of free-particle motion, i.e., the geodesics, are straight lines. In particular, these geodesics can intersect with each other at most once. Therefore, two geodesics can intersect at two points only when the space has a finite curvature.

In two-dimensional systems, this observation is quantitatively formulated with the help of the Gauss-Bonnet theorem. The Gauss-Bonnet theorem relates a closed loop on a curved surface to the Gaussian curvature enclosed by the loop [15, 16]. For a polygon S made of geodesics on a curved surface, the following relation follows from the Gauss-Bonnet theorem:

$$\sum_i \phi_i + K = \sum_i (\pi - \theta_i) + K = 2\pi, \quad (23)$$

where i is the label for the vertices, $\phi_i, \theta_i = \pi - \phi_i$ are the exterior and interior angle at vertex i , and K is the integrated Gaussian curvature enclosed by the polygon:

$$K = \int_S \kappa \sqrt{\det g_{ij}} d^2x. \quad (24)$$

Here, $\kappa = R_{xyxy}/\det g_{ij}$ is the Gaussian curvature and R_{ijkl} is the standard Riemann curvature tensor for the effective metric g_{ij} (see Appendix E). It should be noted that R_{ijkl} can be expressed in terms of the Riemannian curvature of the Hilbert space defined by the quantum metric, as detailed in the Appendix F. For the coplanar texture Eq. (21), this takes the form

$$K = \int d^2x \frac{l_C^2}{4} \frac{(\partial_x^2 \theta)(\partial_y^2 \theta) - (\partial_x \partial_y \theta)^2}{(1 + |l_C \partial_i \theta / 2|^2)^{3/2}}. \quad (25)$$

When the metric is trivial and the curvature vanishes, $K = 0$ and Eq. (23) reduces to the well-known polygon exterior angle sum theorem. On a curved surface, K is finite, and the exterior angle sum will be modified.

We can apply Eq. (23) when two geodesics intersect at two points as in Fig. 3(a), since they can be viewed as a polygon consisting of two edges. In this case, Eq. (23) reduces to

$$\theta_1 + \theta_2 = K. \quad (26)$$

It should be emphasized that θ_i here is the angle measured with the effective metric g_{ij} , and not necessarily equal to the angle we measure in real space with the trivial metric δ_{ij} . In the case of radial spiral, the θ_i are measured on the corresponding cone, as shown in Fig. 3. The curvature vanishes except at the origin, and the origin contributes to K by the angle deficit of the cone: $\kappa = 2\pi(1 - 1/\sqrt{1 + (\pi l_C/\lambda_s)^2})\delta(\mathbf{x})$.

More generally, the deflection angle is related to the curvature. Consider the case where the curved metric (and thus the curvature) is localized in a small region, as shown in Fig. 3(b), and a particle travels from point 1 to point 2 on a geodesic (orange solid line). Since the curved metric is localized, we can also draw a geodesic

connecting the points only through the flat space if the points are sufficiently far away from the curved region. This geodesic is simply a straight line, as shown with a blue line in Fig. 3(c). Then we can define the deflection angle φ as the angle change of the velocity from point 1 to 2 within the flat region. On the other hand, since the orange and blue lines form a geodesic polygon, we can apply Eq. (26). Since the deflection angle is related to θ_1 and θ_2 as $\varphi = \theta_1 + \theta_2$, it follows that

$$\varphi = K. \quad (27)$$

Note that φ here is the angle change of the velocity within the flat space, and thus is defined with the flat metric δ_{ij} . Eq. (27) reveals the geometric nature of the gravitational lensing [17].

For example, we may consider a coplanar texture which varies with wavelength λ_s . Using Eq. (25), we find that over a region of area A , the deflection angle scales as

$$\varphi \sim A l_C^2 / \lambda_s^4. \quad (28)$$

For masses ranging from 0.1 to 1 electron mass and typical 10-100 meV Hund's couplings, $l_C \sim 1$ -10 nm. Meanwhile, typical spin textures have $\lambda_s \sim 10$ -100 nm. Hence the deflection angle from gravitational lensing is within the range of observability over areas $A \sim \lambda_s^2$, and can be enhanced by coherent electron motion across larger samples.

Discussion. — The emergent gravity discussed in this work originates from the quantum nature of electrons. Indeed, the correction to the spatial metric vanishes in the limit of $\hbar \rightarrow 0$. As we discussed with the spiral spin texture, the correction to the metric comes from the suppression of the wavefunction overlap, and thus cannot be understood without quantum mechanical wavefunctions.

Another way to interpret the emergent gravity is in terms of the electron's wave nature. From the wave perspective, the effective metric g determines the electron's wavelength λ for a given frequency ω . Therefore, g essentially plays the role of the refractive index for the electron's quantum mechanical wave. A spatially dependent g corresponds to a spatially dependent refractive index, and thus causes refraction, i.e., the lensing effect. We note that the gravitational lensing effect of light in the true gravity can also be understood with the effective refractive index of light due to gravity [12].

It is important to note that the emergent gravity — and thus the gravitational lensing effect — does not require any symmetry breaking. This contrasts with the emergent magnetic field, which requires the time reversal symmetry breaking. In particular, the gravitational lensing effect can occur without magnetic fields. This is distinct from the conventional electron lensing in electron microscopes [18], where magnetic fields are used to control electrons' trajectory.

A curved space was previously discussed in the context of condensed matter. For example, strain responses were theoretically studied by introducing metric [19–23].

Note that we do *not* consider any strain in this work. The effectively curved space we discussed emerges due to the quantum mechanical coupling between the itinerant electrons' spin and localized spins. A curved space is also used as a theoretical tool to study properties of electronic systems, such as fractional quantum Hall systems [19, 24, 25]. The emergent gravity may provide a method to experimentally test these theoretical results.

The concept of emergent gauge field is so far well established and generically appears in various quantum systems. In these systems, there should always be a correction due to the finite energy gap, which results in emergent gravity. In addition, the emergent gravity requires

no symmetry breaking in contrast to the emergent magnetic field, which relies on time reversal symmetry breaking. Therefore, we expect the emergent gravity to appear in quantum systems ubiquitously.

ACKNOWLEDGMENTS

YO thanks Filippo Gaglioli for encouraging discussion. LF and NP thank Aidan Reddy for participation in a related project. This work was supported by the Air Force Office of Scientific Research under award number FA2386-24-1-4043. LF was supported in part by the Simons Investigator Award from the Simons Foundation.

-
- [1] G. Sundaram and Q. Niu, Wave-packet dynamics in slowly perturbed crystals: Gradient corrections and Berry-phase effects, *Physical Review B* **59**, 14915 (1999), publisher: American Physical Society.
 - [2] D. Loss, P. Goldbart, and A. V. Balatsky, Berry's phase and persistent charge and spin currents in textured mesoscopic rings, *Physical Review Letters* **65**, 1655 (1990).
 - [3] J. Ye, Y. B. Kim, A. J. Millis, B. I. Shraiman, P. Majumdar, and Z. Tešanović, Berry Phase Theory of the Anomalous Hall Effect: Application to Colossal Magnetoresistance Manganites, *Physical Review Letters* **83**, 3737 (1999).
 - [4] Y. Taguchi, Y. Oohara, H. Yoshizawa, N. Nagaosa, and Y. Tokura, Spin Chirality, Berry Phase, and Anomalous Hall Effect in a Frustrated Ferromagnet, *Science* **291**, 2573 (2001).
 - [5] M. Onoda, G. Tatara, and N. Nagaosa, Anomalous Hall Effect and Skyrmin Number in Real and Momentum Spaces, *Journal of the Physical Society of Japan* **73**, 2624 (2004).
 - [6] K. Ohgushi, S. Murakami, and N. Nagaosa, Spin anisotropy and quantum Hall effect in the kagome lattice: Chiral spin state based on a ferromagnet, *Physical Review B* **62**, R6065 (2000), publisher: American Physical Society.
 - [7] P. Bruno, V. K. Dugaev, and M. Taillefer, Topological Hall Effect and Berry Phase in Magnetic Nanostructures, *Physical Review Letters* **93**, 096806 (2004), publisher: American Physical Society.
 - [8] K. Hamamoto, M. Ezawa, and N. Nagaosa, Quantized topological Hall effect in skyrmion crystal, *Physical Review B* **92**, 115417 (2015), publisher: American Physical Society.
 - [9] Z. Addison, L. Keyes, and M. Randeria, Anomalous and Topological Hall Effects with Phase-Space Berry Curvatures: Electric, Thermal, and Thermoelectric Transport in Magnets (2024), arXiv:2409.04376 [cond-mat].
 - [10] T. Park, X. Huang, L. Savary, and L. Balents, Quantum geometry from the Moyal product: quantum kinetic equation and non-linear response (2025), arXiv:2504.10447 [cond-mat].
 - [11] N. Paul, Y. Zhang, and L. Fu, Giant proximity exchange and flat Chern band in 2D magnet-semiconductor heterostructures, *Science Advances* **9**, eabn1401 (2023), publisher: American Association for the Advancement of Science.
 - [12] P. Schneider, J. Ehlers, and E. E. Falco, *Gravitational Lenses*, edited by I. Appenzeller, G. Börner, M. Harwit, R. Kippenhahn, J. Lequeux, P. A. Strittmatter, and V. Trimble, Astronomy and Astrophysics Library (Springer Berlin Heidelberg, Berlin, Heidelberg, 1992).
 - [13] T. Ohnishi and N. Nagaosa, Adiabatic Approximation for Path Integrals and Geometrical Potentials, *Journal of the Physical Society of Japan* **76**, 015003 (2007), publisher: The Physical Society of Japan.
 - [14] S. Deser, R. Jackiw, and G. 't Hooft, Three-dimensional Einstein gravity: Dynamics of flat space, *Ann. Phys.* **152**, 220 (1984).
 - [15] M. Nakahara, *Geometry, Topology and Physics*, 2nd ed. (CRC Press, Boca Raton, 2018).
 - [16] S. Kobayashi, *Differential Geometry of Curves and Surfaces*, Springer Undergraduate Mathematics Series (Springer Singapore, Singapore, 2019).
 - [17] After completing this work, we found a similar relations for the true gravitational lensing of light in Ref. [26].
 - [18] R. Egerton, *Physical Principles of Electron Microscopy* (Springer International Publishing, Cham, 2016).
 - [19] J. E. Avron, R. Seiler, and P. G. Zograf, Viscosity of Quantum Hall Fluids, *Physical Review Letters* **75**, 697 (1995).
 - [20] T. L. Hughes, R. G. Leigh, and E. Fradkin, Torsional Response and Dissipationless Viscosity in Topological Insulators, *Physical Review Letters* **107**, 075502 (2011), publisher: American Physical Society.
 - [21] B. Bradlyn, M. Goldstein, and N. Read, Kubo formulas for viscosity: Hall viscosity, Ward identities, and the relation with conductivity, *Physical Review B* **86**, 245309 (2012).
 - [22] L. Dong and Q. Niu, Geometrodynamics of electrons in a crystal under position and time-dependent deformation, *Physical Review B* **98**, 115162 (2018), publisher: American Physical Society.
 - [23] P. Rao and B. Bradlyn, Hall Viscosity in Quantum Systems with Discrete Symmetry: Point Group and Lattice Anisotropy, *Physical Review X* **10**, 021005 (2020).
 - [24] X. G. Wen and A. Zee, Shift and spin vector: New topological quantum numbers for the Hall fluids, *Physical Re-*

- view Letters **69**, 953 (1992).
- [25] B. Estienne, N. Regnault, and V. Crépel, Ideal Chern bands as Landau levels in curved space, *Physical Review Research* **5**, L032048 (2023).
 - [26] G. W. Gibbons and M. C. Werner, Applications of the Gauss–Bonnet theorem to gravitational lensing, *Classical and Quantum Gravity* **25**, 235009 (2008).

Appendix A: Derivation of the effective Hamiltonian

1. Effective Hamiltonian for general spin textures

Consider the following Hamiltonian:

$$H = \frac{(\mathbf{p} - e\mathbf{A})^2}{2m} - J\mathbf{S}(\mathbf{x}) \cdot \boldsymbol{\sigma} \quad (\text{A1})$$

Here, we include the spatial dependence of J . In this section, assuming J is large, we derive the low-energy effective theory up to $\mathcal{O}(J^{-1})$ by applying the Schrieffer-Wolff transformation.

We first consider the unitary matrix $U(\mathbf{x})$ that diagonalizes the spin:

$$U^\dagger(\mathbf{x})(\mathbf{S}(\mathbf{x}) \cdot \boldsymbol{\sigma})U(\mathbf{x}) = \sigma_z \quad (\text{A2})$$

Then we can obtain Hamiltonian H' in the new basis defined by $U(\mathbf{x})$:

$$H' = U^\dagger(\mathbf{x})HU(\mathbf{x}) = \frac{(\mathbf{p} - e\mathbf{A} - \mathbf{a})^2}{2m} - J\sigma_z \quad (\text{A3})$$

where we set $\hbar = 1$, and \mathbf{a} is defined as

$$\mathbf{a} = U^\dagger(\mathbf{x})i\nabla U(\mathbf{x}) = \begin{pmatrix} \mathbf{a}_{11} & \mathbf{a}_{12} \\ \mathbf{a}_{21} & \mathbf{a}_{22} \end{pmatrix} \quad (\text{A4})$$

and serves as a $U(2)$ gauge field. From now on, we include $(\mathbf{a}_{11} + \mathbf{a}_{22})/2$ in the regular vector potential \mathbf{A} and treat \mathbf{a} as a $SU(2)$ gauge field with $\mathbf{a}_{11} + \mathbf{a}_{22} = 0$. Noting that $\mathbf{a}_{12} = \mathbf{a}_{21}^*$, H' can be written as

$$H' = H_0 + V \quad (\text{A5})$$

where

$$H_0 = \begin{pmatrix} H_1 & 0 \\ 0 & H_2 \end{pmatrix} \quad (\text{A6a})$$

$$V = \begin{pmatrix} 0 & \Lambda \\ \Lambda^\dagger & 0 \end{pmatrix} \quad (\text{A6b})$$

$$\Lambda = -\frac{1}{2m}\{\boldsymbol{\pi}_0, \mathbf{a}_{12}\} \quad (\text{A6c})$$

Here, $H_i = (\boldsymbol{\pi}_i^2 + |\mathbf{a}_{12}|^2)/(2m) \mp J$, $\boldsymbol{\pi}_i = \mathbf{p} - e\mathbf{A} - \mathbf{a}_{ii}$, and $\boldsymbol{\pi}_0 = \mathbf{p} - e\mathbf{A}$. It may be worth noting that Λ has a similar form to the strain generator $J_\nu^\mu \equiv \{x^\mu, p_\nu\}$ [21, 23]. When \mathbf{a}_{12} is linear in the position x^i and $\mathbf{A} = 0$, then Λ coincides with the strain generator up to a factor. For more general \mathbf{a}_{12} , Λ can be interpreted as a generator for a position-dependent strain.

We now apply Schrieffer-Wolff transformation to H' assuming that J is large. We consider a unitary transformation e^S to apply to H' as $H'' = e^S H' e^{-S}$. Assuming that $S = S^{(1)} + S^{(2)} + \dots$ with $S^{(i)} = \mathcal{O}((\Lambda/J)^i)$, H'' is expanded as

$$\begin{aligned} H'' &= H' + [S, H'] + \frac{1}{2}[S, [S, H']] + \dots \\ &= H_0 + V + [S, H_0] + [S, V] + \frac{1}{2}[S, [S, H_0]] + \dots \end{aligned} \quad (\text{A7})$$

We require $S^{(1)}$ to satisfy the following:

$$V + [S^{(1)}, H_0] = 0. \quad (\text{A8})$$

Writing each element explicitly,

$$S_{11}^{(1)} H_1 - H_1 S_{11}^{(1)} = 0, \quad (\text{A9a})$$

$$\Lambda + S_{12}^{(1)} H_2 - H_1 S_{12}^{(1)} = 0, \quad (\text{A9b})$$

$$\Lambda^\dagger + S_{21}^{(1)} H_1 - H_2 S_{21}^{(1)} = 0, \quad (\text{A9c})$$

$$S_{22}^{(1)} H_2 - H_2 S_{22}^{(1)} = 0. \quad (\text{A9d})$$

For the leading order in Λ/J , these can be solved as

$$S_{12}^{(1)} = -S_{21}^{(1)\dagger} = -\frac{\Lambda}{2J}, \quad (\text{A10})$$

$$S_{11}^{(1)} = S_{22}^{(1)} = 0. \quad (\text{A11})$$

Then the effective Hamiltonian for the low energy sector up to $\mathcal{O}(J^{-1})$ is given by $H_{\text{eff}} = H''_{11}$ as

$$\begin{aligned} H_{\text{eff}} &= -J + \frac{\pi_1^2 + |\mathbf{a}_{12}|^2}{2m} - \frac{\Lambda\Lambda^\dagger}{2J} \\ &= -J + \frac{\pi_1^2 + |\mathbf{a}_{12}|^2}{2m} - \frac{\{\boldsymbol{\pi}_0, \mathbf{a}_{12}\}\{\mathbf{a}_{21}, \boldsymbol{\pi}_0\}}{8m^2 J} \end{aligned} \quad (\text{A12})$$

As we discussed in the main text, this effective Hamiltonian is valid when $l_C^2 \ll \lambda_s \lambda_F$ with $l_C \equiv 1/\sqrt{mJ}$, the length scale of the spin texture $\lambda_s \equiv |\nabla \mathbf{S}|^{-1}$, and the Fermi wavelength λ_F .

2. When the spin is slowly varying in space

When the length scale of spatial variation of $\mathbf{S}(\mathbf{x})$, denoted as λ_s , is large so that $\lambda_s \gg \lambda_F$, the derivative of \mathbf{a}_{12} in Eq. (A12) is negligible compared to the other terms. Therefore, we can further simplify Eq. (A12) as

$$\begin{aligned} H_{\text{eff}} &= -J + \frac{\pi_1^2 + |\mathbf{a}_{12}|^2}{2m} - \frac{\pi_{0i} Q_{ij} \pi_{0j}}{2m^2 J} + \mathcal{O}\left(E_F \frac{\lambda_F l_C^2}{\lambda_s^3}\right) \\ &= -J + \frac{\pi_1^2 + |\mathbf{a}_{12}|^2}{2m} - \frac{\pi_{0i} G_{ij} \pi_{0j}}{2m^2 J} - \frac{e\hbar^3}{4m^2 J} \boldsymbol{\Omega} \cdot \mathbf{B} \end{aligned} \quad (\text{A13})$$

where $Q_{ij} = a_{12}^i a_{21}^j$ is the quantum geometric tensor, $G_{ij} = \text{Re } Q_{ij}$, $\Omega_{ij} = -2 \text{Im } Q_{ij}$ are the quantum metric and the Berry curvature respectively, and $\boldsymbol{\Omega}$ is defined as $\Omega^i = \epsilon^{ijk} \Omega_{jk}/2$. E_F is the Fermi energy. Since $\mathbf{a}_{11} = \mathcal{O}(1/\lambda_s)$ and $G_{ij} = \mathcal{O}(1/\lambda_s^2)$, we can replace $\boldsymbol{\pi}_0$ with $\boldsymbol{\pi}_1$ up to the same accuracy of the approximation to obtain

$$\begin{aligned} H_{\text{eff}} &= -J(\mathbf{x}) + \frac{\pi_{1i} g^{ij} \pi_{1j}}{2m} + \frac{\hbar^2 \text{Tr } G}{2m} - \frac{e^3 \hbar}{4m^2 J} \boldsymbol{\Omega} \cdot \mathbf{B} \\ &\quad + \mathcal{O}\left(E_F \frac{\lambda_F l_C^2}{\lambda_s^3}\right) \end{aligned} \quad (\text{A14})$$

Here, $g^{ij} = \delta^{ij} - l_C^2 G_{ij}$ is the effective metric, and $\boldsymbol{\Omega} = \nabla \times \mathbf{a}_{11}$ is the Berry curvature.

Appendix B: Analogy to true gravity

The emergent gravity is an analogue of Einstein gravity in condensed matter. This analogy becomes clearer in the Lagrangian formalism. The Lagrangian corresponding to the Hamiltonian (8) is given by $L = p_i \dot{x}^i - H$ as

$$L(x, \dot{x}) = \frac{m}{2} g_{ij}(\mathbf{x}) \dot{x}^i \dot{x}^j + e \mathcal{A}_i(\mathbf{x}) \dot{x}^i + J - V(\mathbf{x}) \quad (\text{B1})$$

This Lagrangian can be obtained from the following action up to $\mathcal{O}(J^{-1} \lambda_s^{-2})$:

$$S = S_0 + m\tilde{c} \int \sqrt{\tilde{g}_{\mu\nu} dx^\mu dx^\nu} \quad (\text{B2})$$

Here, $S_0 = \int dt (m\dot{x}^2/2 - V + e\mathcal{A}_i \dot{x}^i)$ is the Lagrangian for a particle in a flat space-time with potential V and vector potential \mathcal{A}_i . The second term in Eq. (B2) represents the effect of the emergent gravity, where μ and ν run over 0 to 3, $(x^0, x^1, x^2, x^3) = (\tilde{c}t, x, y, z)$. \tilde{c} is defined through $m\tilde{c}^2 = J$. The space-time metric \tilde{g} is given by

$$\tilde{g}_{\mu\nu} = \begin{pmatrix} 1 & \\ & \frac{\hbar^2}{m^2 \tilde{c}^2} G_{\mu\nu} \end{pmatrix} \quad (\text{B3})$$

Eq. (B2) shows that the correction to our low-energy effective action takes the same form as the action for a particle with the space-time metric \tilde{g} . The role of the rest energy mc^2 in the true gravity with c the speed of light is played by $J = m\tilde{c}^2$ in the emergent gravity, defining an effective speed of light \tilde{c} . The effect from the spatial components of the space time metric gives the correction to the Hamiltonian of order $\mathcal{O}(E_F/(m\tilde{c}^2))$, just as the true gravity effects from the curved space-time scales as $\mathcal{O}(E_K/(mc^2))$ with E_K the kinetic energy of a particle.

Appendix C: Correspondence to other forms of Hamiltonian in a curved space

In the main text, we discuss the effective Hamiltonian in the following form as the Hamiltonian in a curved space:

$$H^{(1)} = \frac{p_i g^{ij} p_j}{2m} + V(\mathbf{x}) \quad (\text{C1})$$

In literature, there is another form of the Hamiltonian which also describes an electron in curved space given by

$$H^{(2)} = \frac{1}{2m} \frac{1}{\sqrt{g}} p_i (\sqrt{g} g^{ij} p_j) + V(\mathbf{x}) \quad (\text{C2})$$

where $g = \det g_{ij}$. The latter is obtained by replacing the Laplacian in the Hamiltonian in flat space with the one in a curved space. In this appendix, we show that these are equivalent up to the accuracy we discussed in the main text.

The most important difference between Eq. (C1) and (C2) is the normalization of the wavefunction $\psi(\mathbf{x})$ they

assume. In the main text, we always assume that the wavefunction is normalized in the following way:

$$\int d^d x |\psi^{(1)}(\mathbf{x})|^2 = 1 \quad (\text{C3})$$

On the other hand, the Hamiltonian $H^{(2)}$ implicitly assumes that the wavefunction is normalized as follows:

$$\int d^d x \sqrt{g} |\psi^{(2)}(\mathbf{x})|^2 = 1 \quad (\text{C4})$$

These two conventions are related as follows: the solution of the Schrodinger equation under $H^{(1)}$, $\psi^{(1)}$, is related to the one under $H^{(2)}$, $\psi^{(2)}$, as $\psi^{(1)} = g^{1/4} \psi^{(2)}$. Since g depends on position in general, the states $\psi^{(1)}$ and $\psi^{(2)}$ and their corresponding Hamiltonian look different from each another.

To show their equivalence, we formulate the Schrodinger equation in a variational way. The Schrodinger equation under Hamiltonian $H^{(i)}$ is obtained from the following action:

$$S^{(1)}[\psi] = \int dt d^d x \left[i\psi^* \frac{\partial \psi}{\partial t} - \frac{1}{2m} (p_i \psi)^* g^{ij} (p_j \psi) - V |\psi|^2 \right] \quad (\text{C5})$$

$$S^{(2)}[\psi] = \int dt d^d x \sqrt{g} \left[i\psi^* \frac{\partial \psi}{\partial t} - \frac{1}{2m} (p_i \psi)^* g^{ij} (p_j \psi) - V |\psi|^2 \right] \quad (\text{C6})$$

where we have set $\hbar = 1$. We find the Schrodinger equation under $H^{(i)}$ by requiring $S^{(i)}$ to be stationary under arbitrary variations of ψ and ψ^* : $\delta S^{(i)}/\delta \psi^* = 0$, and its complex conjugate.

Now we would like to show that $S^{(1)}[g^{1/4}\psi] = S^{(2)}[\psi]$ up to the accuracy we considered in the main text. We start with $S^{(1)}[g^{1/4}\psi]$ and rewrite it as follows:

$$S^{(1)}[g^{1/4}\psi] = \int dt d^d x \sqrt{g} \left[i\psi^* \frac{\partial \psi}{\partial t} - V |\psi|^2 - \frac{1}{2m} (g^{-1/4} p_i g^{1/4} \psi)^* g^{ij} (g^{-1/4} p_j g^{1/4} \psi) \right] \quad (\text{C7})$$

Here, we have assumed g is time-independent. Noting $g^{-1/4} p_i g^{1/4} = p_i - i\alpha_i$ with $\alpha_i = (1/4) \partial_i \log g$, we can rewrite $S^{(1)}[g^{1/4}\psi]$ as

$$\begin{aligned} S^{(1)}[g^{1/4}\psi] &= \int dt d^d x \sqrt{g} \left[i\psi^* \frac{\partial \psi}{\partial t} - V |\psi|^2 - \frac{1}{2m} ((p_i - i\alpha_i) \psi)^* g^{ij} ((p_j - i\alpha_j) \psi) \right] \\ &= S^{(2)}[\psi] + \int dt d^d x \sqrt{g} \frac{1}{2m} (\partial_i \alpha^i - \alpha^i \alpha_i) |\psi|^2 \end{aligned} \quad (\text{C8})$$

where $\alpha^i = g^{ij} \alpha_j$. Eq. (C8) shows that the theory (C1) differs from the theory (C2) only by a correction to a potential, $\delta V = (\partial_i \alpha^i - \alpha^i \alpha_i)/(2m)$.

Lastly, we note that the metric g we considered in the main text is $g_{ij} = \delta_{ij} + \mathcal{O}(l_C^2 \lambda_s^{-2})$ with $l_C = (mJ)^{-1/2}$ the coupling constant and λ_s the length scale of the spin texture. Therefore, $\alpha = \mathcal{O}(l_C^2 \lambda_s^{-3})$ and thus the last term in Eq. (C8) is $\mathcal{O}(l_C^2 \lambda_s^{-4})$. Then we find

$$S^{(1)}[g^{1/4}\psi] = S^{(2)}[\psi] + \mathcal{O}(l_C^2 \lambda_s^{-4}). \quad (\text{C9})$$

Therefore, $H(1)$ and $H^{(2)}$ are equivalent up to $\mathcal{O}(l_C^2 \lambda_s^{-4})$.

Appendix D: Geodesics in spin textures

In this Appendix, we provide more details on the various spin textures explored in the main text and extensions thereof.

1. Radial spiral spin texture

Here, we present details on the radial spiral spin texture

$$\mathbf{S}(\mathbf{x}) = (\cos \frac{2\pi}{\lambda_s} r, \sin \frac{2\pi}{\lambda_s} r, 0), \quad (\text{D1})$$

where $r = \sqrt{x^2 + y^2}$, a simple spin texture with constant real-space quantum metric and $\mathbf{b} = 0$. This combination of features implies that only the emergent gravitational field

$$g^{ij} = \delta^{ij} - \nu \frac{x^i x^j}{r^2}. \quad (\text{D2})$$

enters the electron equation of motion. Here we've defined

$$\nu = (\pi l_C / \lambda_s)^2. \quad (\text{D3})$$

a. Geodesics from direct calculation

The geodesic equation $\ddot{x}^i + \Gamma_{jk}^i \dot{x}^j \dot{x}^k = 0$ reduces to

$$\ddot{\mathbf{x}} = -\nu \mathbf{x} \frac{(\dot{\mathbf{x}} \times \mathbf{x})^2}{x^4}. \quad (\text{D4})$$

In radial coordinates, this is

$$\ddot{\mathbf{r}} = -\nu r \dot{\theta}^2 \hat{\mathbf{r}}. \quad (\text{D5})$$

Comparing with

$$\ddot{\mathbf{r}} = (\ddot{r} - r\dot{\theta}^2)\hat{\mathbf{r}} + \frac{d}{dt}(r^2\dot{\theta})\hat{\boldsymbol{\theta}}, \quad (\text{D6})$$

we find two scalar equations:

$$0 = \frac{d}{dt}(r^2\dot{\theta}) \quad (\text{D7a})$$

$$\ddot{r} = (1 - \nu)r\dot{\theta}^2. \quad (\text{D7b})$$

We may define a conserved angular momentum $h = r^2\dot{\theta} = \text{constant}$. The remaining equation is

$$\ddot{r} = (1 - \nu)h^2/r^3. \quad (\text{D8})$$

Assuming $r(0) = r_0$ and $\dot{r}(0) = v_0$, we have

$$r(t) = \pm \sqrt{(v_0 t + r_0)^2 + (1 - \nu)(ht/r_0)^2}. \quad (\text{D9})$$

We can integrate to find $\theta(t)$ using $\dot{\theta} = h/r^2$. Let $\theta(0) = \theta_0$. We find

$$\begin{aligned} \theta(t) - \theta_0 = & \frac{1}{\sqrt{1 - \nu}} \left(\tan^{-1} \left(\left[\frac{v_0^2}{h\sqrt{1 - \nu}} + \frac{h\sqrt{1 - \nu}}{r_0^2} \right] t + \frac{r_0 v_0}{h\sqrt{1 - \nu}} \right) \right. \\ & \left. - \tan^{-1} \left(\frac{r_0 v_0}{h\sqrt{1 - \nu}} \right) \right) \end{aligned} \quad (\text{D10})$$

This describes a particle on a cone, with the conical singularity at $r = 0$. This geometry also describes the solution of the Einstein equations in the presence of a point mass in (2+1)d with zero cosmological constant [14]. Note that there is no Newtonian attraction; a geodesic at fixed $r(t) = r_0$ is perfectly valid. However, there is "focusing"; two trajectories which pass on either side of the origin will intersect on the other side.

At this point, geodesics depend on the independent parameters (r_0, θ_0, v_0, h) . Another useful form is in terms of $(r_0, \theta_0, v_i, \phi_0)$ where

$$\mathbf{v}_i = v_i (\cos \phi_0, \sin \phi_0) \quad (\text{D11})$$

is the initial Cartesian velocity. The conserved angular momentum is

$$h = r_0 v \sin(\phi_0 - \theta_0), \quad (\text{D12})$$

while the initial radial velocity v_0 satisfies

$$v_0^2 = v_i^2 \cos^2(\phi_0 - \theta_0). \quad (\text{D13})$$

We rescale time $t \mapsto t/v_i$ in the following, which omits explicit dependence on velocity. Defining the angle difference

$$\vartheta_0 = \phi_0 - \theta_0, \quad (\text{D14})$$

the geodesics are

$$\begin{aligned} r(t) &= \pm \sqrt{(r_0 + t \cos \vartheta_0)^2 + (1 - \nu)t^2 \sin^2(2\vartheta_0)/4} \\ \theta(t) - \theta_0 &= \frac{1}{\sqrt{1 - \nu}} (\tan^{-1}(\gamma t + \delta) - \tan^{-1} \delta) \end{aligned} \quad (\text{D15})$$

where

$$\begin{aligned} \gamma &= -\frac{\cot(\vartheta_0)}{2\sqrt{1 - \nu}r_0} ((1 - \nu) \cos(2\vartheta_0) + \nu - 3) \\ \delta &= \frac{\csc \vartheta_0}{\sqrt{1 - \nu}}. \end{aligned} \quad (\text{D16})$$

Example geodesics are plotted in Fig. 4 for $\nu = 0.3$.

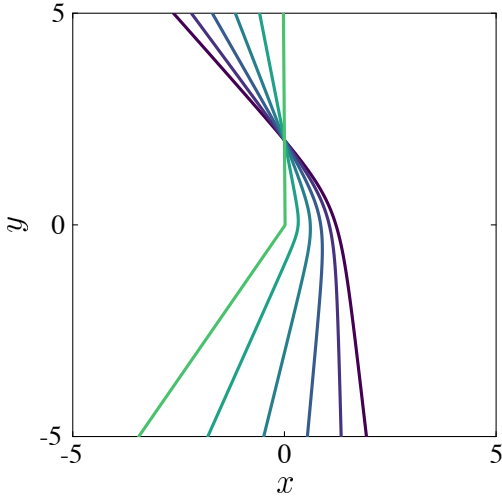


FIG. 4. Example geodesics of the cone geometry with $\nu = 0.3$ (corresponding to a deficit angle $\approx 0.24\pi$) from Eq. (D15). These satisfy $r_0 = 2, \theta_0 = \pi/2$, and varying ϕ_0 . As the geodesics approach the origin, they become the union of two rays.

b. Geodesics from trivial coordinates

Alternatively, we can solve the geodesic equation for the radial spiral spin texture by taking coordinates in which the metric is trivial. To find such coordinates, we start with the effective line element for the radial spiral:

$$dl^2 = dx^2 + dy^2 + dz_{\text{eff}}^2, \quad (\text{D17})$$

where z_{eff} is the embedding coordinate. For the radial spiral, $z_{\text{eff}} = \frac{\pi l_C}{\lambda_s} r$ where $r = \sqrt{x^2 + y^2}$. Therefore, in the polar coordinates (r, θ) with $r \geq 0, 0 \leq \theta < 2\pi$, the line element is given by

$$dl^2 = \left(\frac{dr}{1-\alpha} \right)^2 + r^2 d\theta^2, \quad (\text{D18})$$

where $\alpha = 1 - 1/\sqrt{1 + (\pi l_C/\lambda_s)^2}$. Then we can see that the metric is trivial in a coordinate $(R, \Theta) = (r/(1-\alpha), (1-\alpha)\theta)$. In this new coordinate, the line element becomes

$$dl^2 = dR^2 + R^2 d\Theta = dX^2 + dY^2, \quad (\text{D19})$$

where $X = R \cos \Theta, Y = R \sin \Theta$. Therefore, in these new coordinates (R, Θ) or (X, Y) , the metric is that of a flat space. Note that Θ now only takes values between $0 \leq \Theta < 2\pi(1-\alpha)$ with angle deficit $\Delta\Theta \equiv 2\pi\alpha$. Intuitively, the effective curved space of a radial spiral is equivalent to a cone, and (X, Y) is the coordinate on the cone's net. Correspondingly, the deficit of Θ from 2π , $\Delta\Theta$, is the angle deficit of the cone (also see Fig. 5).

Since the metric in (X, Y) coordinates is trivial, the trajectory of a particle is a straight line with constant

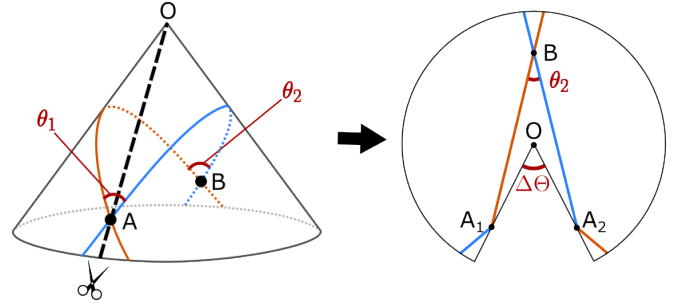


FIG. 5. Geodesics on a cone and the corresponding net. The left panel shows geodesics on the cone intersecting at points A and B, with interior angles θ_1 and θ_2 . The right panel shows the net obtained by cutting the cone along line OA, where points A_1 and A_2 both represent the same point A on the cone. The angle $\Delta\Theta$ denotes the cone's angle deficit.

velocity in (X, Y) coordinates: $\mathbf{X}(t) = \mathbf{X}_0 + \mathbf{V}t$. Such straight lines can be expressed with R, Φ as

$$R \cos(\Theta - \Theta_0) = \text{const.} \quad (\text{D20})$$

with a constant Θ_0 . Rewriting this with r, θ coordinates, we find

$$r \cos((1-\alpha)(\theta - \theta_0)) = \text{const.} \quad (\text{D21})$$

When a particle comes from $r = \infty$ at $t = -\infty$, passes by around the origin and goes to $r = \infty$ at $t = +\infty$, θ at $t = \pm\infty$ has to satisfy either $(1-\alpha)(\theta - \theta_0) = \pm\pi/2$. Therefore, θ at $t = \pm\infty$ is either $\theta_{\pm} = \pm\frac{\pi}{2(1-\alpha)} + \theta_0$. In particular, the deflection angle φ is given by:

$$|\varphi| = \pi - (\theta_+ - \theta_-) = \frac{\pi\alpha}{1-\alpha}. \quad (\text{D22})$$

This deflection angle is clearly seen in Fig. 4.

We can also confirm Eq. (26) in the main text for the radial spiral by considering the geodesics on the cone's net. Consider when two geodesics intersect at two points A and B with interior angles θ_1 and θ_2 , as illustrated in the left panel of Fig. 5. We can obtain the corresponding net by cutting the cone along line OA, which is shown in the right panel. Noting that the sum of the interior angles of a polygon OA_2BA_1 is 2π and that $\angle OA_1B + \angle OA_2B = \theta_1$, we find $\Delta\Theta = \theta_1 + \theta_2$. Since the integrated Gaussian curvature K enclosed by the two geodesics is nothing but the angle deficit $\Delta\Theta$, we confirm $\theta_1 + \theta_2 = K$. We also note that Eq. (27) does not apply to the current case, because the curved metric in the radial spiral is not localized as we assumed in deriving Eq. (27).

While the deflection of geodesics in a curved space is qualitatively different than scattering off of a potential, we may note the following: deflection of geodesics in the cone geometry, and indeed any geometry with positive Gaussian curvature, resembles scattering due to a potential well, while deflection due to a negative curvature would resemble scattering off of a potential barrier. This follows from the Gauss-Bonnet theorem: when curvature

is positive, a pair of geodesics can close to form a polygon, while when the curvature is negative this is not possible. When electrons scatter due to a localized spin texture (outside of which spins are uniform), the potential V always acts as a barrier, while the emergent metric may scatter electrons in a manner resembling either a potential barrier or well (with Fig. 4 depicting the latter).

c. Other properties of the radial spiral spin texture

Let us discuss two properties of the radial spiral spin texture: (1) uniqueness properties and (2) approximation of realistic spin textures obtained from minimizing spin gradient energy.

Uniqueness. The radial spiral is the unique spin spiral which is coplanar, continuous, rotationally symmetric, and has constant squared gradient $\sum_i (\partial_i \mathbf{S})^2$. In fact, this is true for the analog of the radial spiral in higher than two dimensions as well, though here we prove it for $d = 2$. Uniqueness here is implicitly up to a spatially constant rotation in spin space, $\mathbf{S}(\mathbf{x}) \mapsto R\mathbf{S}(\mathbf{x})$ where $R \in SO(3)$.

To prove this, first let us apply a rotation so that $\mathbf{S} \cdot \hat{z} = 0$. Then we can assume

$$\mathbf{S}(\mathbf{x}) = (\cos f(r), \sin f(r), 0) \quad (\text{D23})$$

in order to maintain $|\mathbf{S}| = 1$ and rotational symmetry. Then $f''(r) = \text{constant}$, which implies $f(r) = ar + b$, and we may assume $b = 0$ by applying an appropriate rotation.

Minimizing spin gradient energy. In the main text, we mentioned that the radial spiral approximately describes configurations minimizing the spin gradient energy in geometries with radial boundary conditions $\mathbf{S}(r_{\min}) \neq \mathbf{S}(r_{\max})$. Here, we explain this further.

Consider the problem of finding the normalized spin texture $\mathbf{S}(\mathbf{x})$ which minimizes the spin gradient energy

$$E[\mathbf{S}] = \frac{K}{2} \int_{\Omega} [d\mathbf{x}] (\partial_i \mathbf{S})^2 \quad (\text{D24})$$

in a disk Ω with radius r_{\max} subject to the following boundary conditions: $\mathbf{S}(r = r_{\max}) = \mathbf{S}_1$ and $\mathbf{S}(r \leq r_{\min}) = \mathbf{S}_0$ for some $r_{\min} < r_{\max}$. For instance, this could describe a region of a ferromagnet outside of which spins point up, but inside of which spins are forced to point in-plane due to a local Zeeman field.

Minimum energy configurations wind only in the $\mathbf{S}_1, \mathbf{S}_0$ plane. Without loss of generality, we assume $\mathbf{S}_1 = \hat{y}$, $\mathbf{S}_0 = \hat{x}$, and take (for two dimensions)

$$\mathbf{S}(\mathbf{x}) = (\cos f(r, \theta), \sin f(r, \theta), 0). \quad (\text{D25})$$

The energy density is $(\partial_r f)^2 + r^{-2}(\partial_\theta f)^2$. Since θ -dependence only increases energy, we take $f(r, \theta) = f(r)$ and find $E[\mathbf{S}] = \frac{K}{2} \int_{r_{\min}}^{r_{\max}} dr r (\partial_r f)^2$. From the Euler-Lagrange equation $\partial_r(r \partial_r f) = 0$ it follows that $f(r) =$

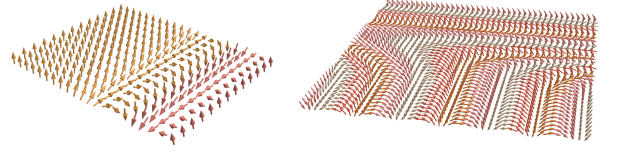


FIG. 6. Left: the spin texture of Eq. (D28). Right: the spin texture of Eq. (D40).

$a \ln r + b$, and matching boundary conditions yields

$$f(r) = \frac{\pi}{2} \frac{\ln(r/r_{\min})}{\ln(r_{\max}/r_{\min})}. \quad (\text{D26})$$

At any radius $r_{\min} < r_* < r_{\max}$, $f(r)$ can of course be locally approximated to linear order as

$$f(r) \approx \frac{\pi}{2} \frac{\ln(r_*/r_{\min})}{\ln(r_{\max}/r_{\min})} + \frac{\pi}{2r_* \ln(r_{\max}/r_{\min})} (r - r_*) \quad (\text{D27})$$

and agrees with the radial spiral. The analogous energy minimization problem in d dimensions yields $f(r) \sim r^{2-d}$, and a linear approximation once again is valid locally, agreeing with the radial spiral. In this sense, the radial spiral *locally* describes an energy minimizing configuration with appropriate radial boundary conditions.

2. Ferromagnet/ spin-helical domain wall

We expand upon the discussion of the transition between ferromagnet and spin-helical regions in the main text. This is a simple setup which captures the bending of geodesics. We take

$$\begin{aligned} \mathbf{S}(\mathbf{x}) &= (0, \sin f(\mathbf{x}), \cos f(\mathbf{x})) \\ f(\mathbf{x}) &= f(x) = \begin{cases} 0 & x \rightarrow -\infty \\ \frac{2\pi x}{\lambda_s} & x \rightarrow +\infty \end{cases} \end{aligned} \quad (\text{D28})$$

We plot this in Fig. 6. This sort of texture could arise in a material with a natural tendency to a helical phase (e.g. with the DMI) and a ferromagnet phase (strong Zeeman field) near a first-order transition; or in the helical phase with an inhomogeneous Zeeman field which turns one side of the material into a ferromagnet.

It is straightforward to see that geodesics will bend across the boundary $x = 0$. The metric is

$$g^{ij} = \delta^{ij} - \frac{l_C^2}{4} f'(x)^2 \delta^{ix} \delta^{jx}. \quad (\text{D29})$$

Geodesics conserve the energy

$$E = \frac{1}{2} m g_{ij} \dot{x}^i \dot{x}^j. \quad (\text{D30})$$

To see this, note that

$$\begin{aligned}
\dot{E}/m &= \frac{1}{2}\dot{x}^k \partial_k g_{ij} \dot{x}^i \dot{x}^j + g_{ij} \ddot{x}^i \dot{x}^j \\
&= \frac{1}{2}\dot{x}^k (\Gamma_{ki}^m g_{mj} + \Gamma_{kj}^m g_{mi}) \dot{x}^i \dot{x}^j + g_{ij} \ddot{x}^i \dot{x}^j \\
&= (g_{ij} \ddot{x}^i + \Gamma_{ki}^m g_{mj} \dot{x}^k \dot{x}^i) \dot{x}^j \\
&= \dot{x}^j g_{rj} (\ddot{x}^r + \Gamma_{ki}^r \dot{x}^k \dot{x}^i) \\
&= 0.
\end{aligned} \tag{D31}$$

Hence

$$E = \frac{1}{2}m \left(1 + \frac{1}{4}l_C^2 f'(x)^2 \right) \dot{x}^2 + \frac{1}{2}m\dot{y}^2 = \text{const.} \tag{D32}$$

Because the system has a y translation invariance, $p_y = mg_{yi}\dot{x}^i$ is conserved. Hence \dot{y} is constant and also

$$\left(1 + \frac{1}{4}l_C^2 f'(x)^2 \right) \dot{x}^2 = \text{const.} \tag{D33}$$

Let $v_{L/R}$ denote the x -velocity for $x \rightarrow \mp\infty$. It follows that

$$\left(1 + \frac{\pi^2 l_C^2}{\lambda_s^2} \right) v_R^2 = v_L^2 \tag{D34}$$

giving us the relation

$$\frac{v_R}{v_L} = \frac{1}{\sqrt{1 + (\pi l_C/\lambda_s)^2}}. \tag{D35}$$

Let $\theta_{L/R}$ be the angle of the geodesic with respect to the x axis in the left and right regions, respectively. It follows that

$$\frac{\tan \theta_R}{\tan \theta_L} = \sqrt{1 + (\pi l_C/\lambda_s)^2}. \tag{D36}$$

While this agrees with Snell's law $\sin \theta_L / \sin \theta_R = n_R / n_L$ for light traveling between two isotropic media with indices of refraction $n_{L/R}$ for *small* angles $\theta_{L/R}$, it differs for larger angles. This distinction has the important consequence that there is no condition for total internal reflection for the relation above.

So far, we've been ignoring the effect of $V(\mathbf{x}) = \hbar^2 f'(x)^2/2m$. If we include the effect of V , the geodesics instead conserve the energy

$$E = \frac{1}{2}mg_{ij}\dot{x}^i\dot{x}^j + V \tag{D37}$$

and following the same steps,

$$\frac{1}{2} \left(1 + (\pi l_C/\lambda_s)^2 \right) v_R^2 + \frac{\hbar^2}{2m^2\lambda_s^2} = \frac{1}{2}v_L^2. \tag{D38}$$

The resulting relation between asymptotic angles is modified to

$$\frac{v_R}{v_L} = \frac{\tan \theta_L}{\tan \theta_R} = \frac{\sqrt{1 - \frac{\hbar^2}{m^2\lambda_s^2 v_L^2}}}{\sqrt{1 + \frac{\pi^2 l_C^2}{\lambda_s^2}}}. \tag{D39}$$

Hence both V and g^{ij} contribute to the bending of trajectories. We can isolate the effect from g^{ij} by considering a domain wall between two distinct spiral phases, which we turn to next.

3. Spiral / spiral domain wall

Consider a spin texture which interpolates between two distinct spiral phases with wavevectors $\mathbf{q}_L = q\hat{x}$ and $\mathbf{q}_R = q\hat{y}$ as x goes from $-\infty$ to $+\infty$. This could capture a domain wall in a chiral magnet which has multiple degenerate ground state spiral solutions. Concretely, consider

$$\mathbf{S}(\mathbf{x}) = (0, \sin \mathbf{q}(x) \cdot \mathbf{x}, \cos \mathbf{q}(x) \cdot \mathbf{x})$$

$$\mathbf{q}(x) = \begin{cases} \frac{2\pi}{\lambda_s} \hat{x} & x \rightarrow -\infty \\ \frac{2\pi}{\lambda_s} \hat{y} & x \rightarrow +\infty \end{cases} \tag{D40}$$

as shown, for instance, in Fig. 6. The metric far to the left and far to the right takes the form

$$\begin{aligned}
g_L^{ij} &= \delta^{ij} - \frac{\pi^2 l_C^2}{\lambda_s^2} \delta^{ix} \delta^{jx} \\
g_R^{ij} &= \delta^{ij} - \frac{\pi^2 l_C^2}{\lambda_s^2} \delta^{iy} \delta^{jy}
\end{aligned} \tag{D41}$$

while $V(\mathbf{x}) = \hbar^2/2m\lambda_s^2$ in both cases. Therefore we can ignore the effect of $V(\mathbf{x})$ for the asymptotic behavior of geodesics and proceed by studying the conserved energy $E = \frac{1}{2}mg_{ij}\dot{x}^i\dot{x}^j$. In the asymptotic regions, we have

$$\begin{cases} (1 + (\pi l_C/\lambda_s)^2) \dot{x}^2 + \dot{y}^2 = C & x \rightarrow -\infty \\ (1 + (\pi l_C/\lambda_s)^2) \dot{y}^2 + \dot{x}^2 = C & x \rightarrow +\infty \end{cases} \tag{D42}$$

with C a constant. Assuming the metric globally only depends on x , the y momentum $p_y = mg_{yi}\dot{x}^i$ is conserved. In the asymptotic regions, we have

$$\begin{cases} p_y = m\dot{y} & x \rightarrow -\infty \\ p_y = m(1 + (\pi l_C/\lambda_s)^2)\dot{y} & x \rightarrow +\infty. \end{cases} \tag{D43}$$

Let us parameterize

$$(\dot{x}, \dot{y}) = \begin{cases} v_L(\cos \theta_L, \sin \theta_L) & x \rightarrow -\infty \\ v_R(\cos \theta_R, \sin \theta_R) & x \rightarrow +\infty \end{cases} \tag{D44}$$

in the asymptotic regions, and for convenience let

$$\nu = (\pi l_C/\lambda_s)^2. \tag{D45}$$

Solving the system of equations yields

$$\tan \theta_R = \frac{\tan \theta_L}{\sqrt{(1 + \nu)^3 + \nu(1 + \nu) \tan^2 \theta_L}}. \tag{D46}$$

This relation is plotted in Fig. 7. To leading order and at small angles, we have

$$\theta_R - \theta_L \approx -\frac{3}{2}\theta_L \frac{\pi^2 l_C^2}{\lambda_s^2}. \tag{D47}$$

Appendix E: Summary of Riemannian geometry

In this Appendix, we summarize the results from Riemannian geometry used in the main text. For a thorough description of the Riemannian geometry, see, for example, Ref. [15, 16].

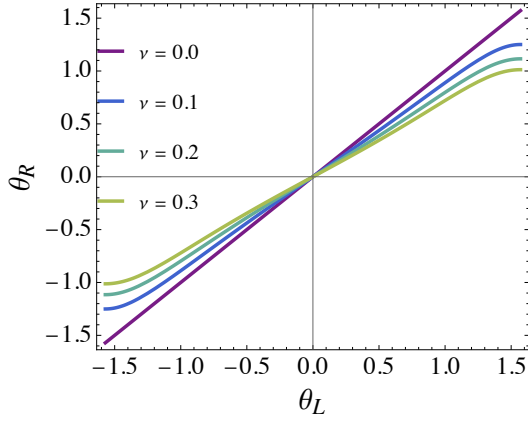


FIG. 7. Plot of Eq. (D46) for a geodesic across a spiral / spiral domain wall.

1. Basics of Riemannian geometry

Consider d -dimensional Riemannian manifold M . The line element on M defines the metric g_{ij} as

$$dl^2 = g_{ij} dx^i dx^j, \quad (E1)$$

where $x^i (i = 1, \dots, d)$ is the (local) coordinate. The metric defines the inner product between vectors A and B , which we denote as $g(A, B) \equiv g_{ij} A^i B^j$. We can define the Levi-Civita connection associated with the metric g_{ij} . The corresponding Christoffel symbol is given by

$$\Gamma_{jk}^i = \frac{g^{im}}{2} (\partial_k g_{mj} + \partial_j g_{mk} - \partial_m g_{jk}), \quad (E2)$$

where $\partial_i = \partial/\partial x^i$. With the Christoffel symbol, we can define the covariant derivative of vectors. For a vector A , its covariant derivative in i -direction, $\nabla_i A$, is given by

$$(\nabla_i A)^j = \partial_i A^j + \Gamma_{ik}^j A^k. \quad (E3)$$

The Riemann curvature tensor R_{ijkl}^i is defined as follows. We denote the basis vector in i -direction as e_i . e_i is what is identified with the partial derivative ∂_i in mathematics literature. R_{ijkl}^i is then defined through the following relation:

$$[\nabla_k, \nabla_l] e_j = R_{jkl}^i e_i. \quad (E4)$$

We can show R_{ijkl}^i is written with the Christoffel symbol as

$$R_{jkl}^i = \partial_k \Gamma_{lj}^i - \partial_l \Gamma_{kj}^i + \Gamma_{km}^i \Gamma_{lj}^m - \Gamma_{lm}^i \Gamma_{kj}^m. \quad (E5)$$

2. Gauss-Bonnet theorem

Here we assume $d = 2$. Gauss-Bonnet theorem relates a closed loop on a two-dimensional curved surface

to the Gaussian curvature enclosed by the loop. Consider a closed loop C , parameterized by its arclength s as $x^i(s)$. C is parameterized so that the vector $\dot{x} \equiv dx/ds$ rotates in counterclockwise. C can have vertices with an exterior angle ϕ_i . Then the Gauss-Bonnet theorem states that the following relation holds for a closed loop C :

$$\int_C k_g ds + \int_S \kappa \sqrt{\det g_{ij}} d^2x + \sum_i \phi_i = 2\pi \chi(S). \quad (E6)$$

Here, S is the region enclosed by C and $\chi(S)$ is the Euler characteristic. κ is the Gaussian curvature, given by

$$\kappa = \frac{R_{xyxy}}{\det g_{ij}}, \quad (E7)$$

where $R_{ijkl} = g_{im} R_{jkl}^m$. k_g is the geodesic curvature of the curve C , defined as

$$k_g = g(\nabla_s \dot{x}, a). \quad (E8)$$

Here, $\dot{x} = dx/ds$ is the tangent vector along the curve C . Since s is the arclength, \dot{x} is a unit vector: $g(\dot{x}, \dot{x}) = 1$. a is a unit vector orthogonal to \dot{x} , satisfying $g(\dot{x}, a) = 0$, $g(a, a) = 1$. As we consider a two-dimensional surface, a is unique up to sign, and we fix the sign so that (\dot{x}, a) forms a local right-handed basis. $(\nabla_s \dot{x})^i = \ddot{x}^i + \Gamma_{jk}^i \dot{x}^j \dot{x}^k$ is the covariant derivative of \dot{x} along the curve, with $\ddot{x}^i = d^2 x^i / ds^2$. Since $\nabla_s \dot{x}$ vanishes when C is a geodesic, k_g also vanishes for a geodesic. Therefore, k_g measures the deviation of the curve from geodesics.

When C is a polygon made of geodesics, $\chi(S) = 1$ and $k_g = 0$. Therefore, it follows

$$\int_S \kappa \sqrt{\det g_{ij}} d^2x + \sum_i \phi_i = 2\pi. \quad (E9)$$

This is what we used in the main text.

Appendix F: Relation to the quantum geometry

In this Appendix, we briefly comment on the relation between the emergent curved space and the quantum geometry.

As discussed in the main text, the emergent curved space is characterized by the effective metric given by $g_{ij} = \delta_{ij} + l_C^2 G_{ij}$, with G_{ij} the quantum metric. On the other hand, the quantum metric G_{ij} defines the Riemannian geometry of the Hilbert space, which we here call *quantum Riemannian geometry*. In the same way as the standard Riemannian geometry, we can define the Christoffel symbol and the Riemann curvature as:

$$\gamma_{jk}^i = \frac{(G^{-1})^{im}}{2} (\partial_k G_{mj} + \partial_j G_{mk} - \partial_m G_{jk}), \quad (F1)$$

$$r_{jkl}^i = \partial_k \gamma_{jl}^i - \partial_l \gamma_{kj}^i + \gamma_{km}^i \gamma_{lj}^m - \gamma_{lm}^i \gamma_{kj}^m. \quad (F2)$$

r_{jkl}^i represents the curvature of the Hilbert space, and we may call the quantum Riemann curvature tensor. We

assume here that G_{ij} is positive definite so that we can define its inverse G^{-1} .

In this case, the Riemann curvature of the emergent space, R_{ijkl} , is directly related to the quantum Riemann

curvature, r_{ijkl} :

$$R^i_{jkl} = l_C^2 r^i_{jkl}. \quad (\text{F3})$$